Charmonia production in p+p collisions under NRQCD formalism

Vineet Kumar[1] and Prashant Shukla[1,2,*]

[1]*Nuclear Physics Division, Bhabha Atomic Research Center, Mumbai, India*

[2]*Homi Bhabha National Institute, Anushakti Nagar, Mumbai, India*

(Dated: June 29, 2016)

Abstract

This work presents the differential charmonia production cross sections in high energy p+p collisions calculated using NRQCD formalism. The NRQCD formalism, factorizes the quarkonia production cross sections in terms of short distance QCD cross sections and long distance matrix elements (LDMEs). The short distance cross sections are calculated in terms of perturbative QCD and LDMEs are obtained by fitting the experimental data. Measured transverse momentum distributions of χ_c, $\psi(2S)$ and J/ψ in p +$\bar{\text{p}}$ collisions at $\sqrt{s} = 1.8$, 1.96 TeV and in p+p collisions at $\sqrt{s} = 7$, 8 and 13 TeV are used to constrain LDMEs. The feed-down contribution to each state from the higher states are taken into account. The formalism provides a very good description of the data in a wide energy range. The values of LDMEs are used to predict the charmonia cross sections in p+p collisions at 13 and 5 TeV in kinematic bins relevant for the LHC detectors. Charmonia ratios are predicted at 1.8, 5 and 13 TeV p+p collisions.

---

[*] pshukla@barc.gov.in

I. INTRODUCTION

The quarkonia ($Q\bar{Q}$) have provided useful tools for probing both perturbative and non-perturbative aspects of Quantum Chromodynamics (QCD) eversince the discovery of J/ψ resonance [1, 2]. The Quarkonia states are qualitatively different from most other hadrons since the velocity v of the heavy constituents is small allowing a non-relativistic treatment of bound states. The quarkonia are the richest probes to study the bulk strongly interacting matter produced in heavy ion collisions [3]. The ratios of excited to ground state quarkonia yields are considered as robust signals of Quark Gluon Plasma (QGP) and measuring such ratios has become the most important goals of Pb+Pb experiments at LHC [4, 5]. The heavy quarks due to their high mass ($m_c \sim 1.6\,\mathrm{GeV/c^2}$, $m_b \sim 4.5\,\mathrm{GeV/c^2}$), are produced in initial partonic collisions with sufficiently high momentum transfers. Thus the heavy quark production can be treated perturbatively [6, 7]. The formation of quarkonia out of the two heavy quarks is a nonperturbative process and is treated in terms of different models [8–10]. Most notable models for quarkonia production are the color-singlet model (CSM), the color-evaporation model (CEM), the non-relativistic QCD (NRQCD) factorization approach, and the fragmentation-function approach.

In the CSM [11–14], it is assumed that the $Q\bar{Q}$ pair that evolves into the quarkonium is in a color-singlet state and has the same spin and angular-momentum as the quarkonium. The production rate of quarkonium state is related to the absolute values of the color-singlet $Q\bar{Q}$ wave function and its derivatives, evaluated at zero $Q\bar{Q}$ separation. These quantities can be extracted by comparing calculated quarkonium decay rates in the CSM with the experimental measurements. The CSM was successful in predicting quarkonium production rates at relatively low energy [15] but, at high energies, very large corrections appear at next-to-leading order (NLO) and next-to-next-to-leading order (NNLO) in α_s [16–18]. The NRQCD factorization approach comprise the color-singlet model, but also includes color-octet states. In the CEM [19–21], it is assumed that the produced $Q\bar{Q}$ pair evolves into a quarkonium if its invariant mass is less than the threshold for producing a pair of open-flavor heavy mesons. The nonperturbative probability for the $Q\bar{Q}$ pair to evolve into a quarkonium state is fixed by comparison with the measured production cross section of that quarkonium state. The CEM calculations provide good descriptions of the CDF data for J/ψ, ψ(2S), and χ_c production at $\sqrt{s} = 1.8$ TeV [21] but it fails to predict the quarkonium polarization.

In the NRQCD factorization approach [8], the probability for a $Q\bar{Q}$ pair to evolve into a quarkonium is expressed as matrix elements of NRQCD operators in terms of the heavy-quark velocity v in the limit $v \ll 1$. This approach takes into account the complete structure of the $Q\bar{Q}$ Fock space, which is spanned by the state $n = {}^{2S+1}L_J^{[a]}$ with spin S, orbital angular momentum L, total angular momentum J, and color multiplicity $a = 1$ (color-singlet), 8 (color-octet). The $Q\bar{Q}$ pairs which are produced at short distances in color-octet (CO) states, evolve into physical, color-singlet (CS) quarkonia by emitting soft gluons nonperturbatively. In the limit $v \to 0$, the CSM is recovered in the case of S-wave quarkonia. The short distance cross sections can be calculated within the framework of perturbative QCD (pQCD). The long distance matrix elements (LDME) corresponding to the probability of the $Q\bar{Q}$ state to convert to the quarkonium can be estimated by comparison with the experimental measurements. The leading order (LO) NRQCD gives a good description of J/ψ yields at RHIC, Tevatron and LHC energies [22].

The NLO corrections to color-singlet J/ψ production have been investigated in Refs. [17, 23]. The color-singlet J/ψ production is found to be enhanced by 2-3 order of magnitude in high p_T region [23]. The NLO corrections to J/ψ production via S-wave color octet (CO) states (${}^1S_0^{[8]}\,{}^3S_1^{[8]}$) are studied in Ref. [24] and the corrections to p_T distributions of both J/ψ yield and polarization are found to be small. In Refs. [25], NLO corrections for χ_{cJ} hadroproduction are also studied.

Several NLO calculations are performed to obtain the polarization and yield of J/ψ. The J/ψ polarization presents a rather confusing pattern [26–28]. The works of Ref. [29] and Ref. [30] present NLO-NRQCD calculations of J/ψ yields. In both the works, the set of CO LDMEs fitted to p_T distributions measured at HERA and CDF are used to describe the p_T distributions from RHIC and the LHC. The fitted LDMEs of Ref. [29] and Ref. [30] are incompatible with each other. A recent work [31] gives calculations for both the yields and polarizations of charmonia at the Tevatron and the LHC where the LDMEs are obtained by fitting the Tevatron data only. With the LHC running for several years we now have very high quality quarkonia production data in several kinematic regions up to very high transverse momentum which could be used to constrain the LDMEs. In this paper, we use CDF data [32–35] along with new LHC data [36–40], [41–44] to constrain the LDMEs. The feed-down contribution to each state from the higher states are taken into account. These new LDMEs are then used to predict the J/ψ and $\psi(2S)$ cross-section at 13 TeV and 5

3

TeV for the kinematical bins relevant to LHC detectors. The NLO calculations are still evolving and thus we use LO calculations in this work. The values of fitted LDMEs with LO formulations are always useful for straightforward predictions of quarkonia cross section and for the purpose of a comparison with those obtained using NLO formulations. The uncertainties in the LDMEs due to NLO are quantified. We also give predictions for the $\psi(2S)$ to J/ψ ratios at $\sqrt{s} = 5$ TeV which has become important due to the recent Pb+Pb collisions at $\sqrt{s_{NN}} = 5$ TeV.

II. QUARKONIA PRODUCTION IN P+P COLLISIONS

The NRQCD formalism provides a theoretical framework for studying the heavy quarkonium production. The dominant processes in the production of heavy mesons ψ are $g + q \to \psi + q$, $q + \bar{q} \to \psi + g$ and $g + g \to \psi + g$. We represent these processes by $a + b \to \psi + X$, where a and b are the light incident partons. The invariant cross-section for the production of ψ can be written in a factorized form as

$$E\frac{d^3\sigma^\psi}{d^3p} = \sum_{a,b} \int \int dx_a\, dx_b\, G_{a/p}(x_a, \mu_F^2)\, G_{b/p}(x_b, \mu_F^2)\, \frac{\hat{s}}{\pi}\frac{d\sigma}{d\hat{t}} \times \delta(\hat{s} + \hat{t} + \hat{u} - M^2), \quad (1)$$

where $G_{a/p}(G_{b/p})$ is the distribution function (PDF) of the incoming parton $a(b)$ in the incident proton, which depends on the momentum fraction $x_a(x_b)$, the factorization scale μ_F. The parton level Mandelstam variables $\hat{s}$, $\hat{t}$, and $\hat{u}$ can be expressed in terms of x_a, x_b as

$$\hat{s} = x_a\, x_b\, s$$
$$\hat{t} = M^2 - x_a\, \sqrt{s}\, m_T\, e^{-y} \quad (2)$$
$$\hat{u} = M^2 - x_b\, \sqrt{s}\, m_T\, e^{y},$$

where $\sqrt{s}$ being the total energy in the centre-of-mass, y is the rapidity and p_T is the transverse momentum of the $Q\bar{Q}$ pair. The mass of heavy meson is repersented by M and m_T is the transverse mass defined as $m_T^2 = p_T^2 + M^2$. Writing down $\hat{s} + \hat{t} + \hat{u} - M^2 = 0$ and solving for x_b we obtain

$$x_b = \frac{1}{\sqrt{s}}\frac{x_a\, \sqrt{s}\, m_T\, e^{-y} - M^2}{x_a\, \sqrt{s} - m_T\, e^{y}}. \quad (3)$$

The double differential cross-section upon p_T and y then is obtained as

$$\frac{d^2\sigma^\psi}{dp_T\, dy} = \sum_{a,b} \int_{x_a^{min}}^1 dx_a\, G_{a/A}(x_a, \mu_F^2)\, G_{b/B}(x_b, \mu_F^2) \times 2p_T\frac{x_a\, x_b}{x_a - \frac{m_T}{\sqrt{s}}e^y}\frac{d\sigma}{d\hat{t}}, \quad (4)$$

4

where the minimum value of x_a is given by

$$x_{a\min} = \frac{1}{\sqrt{s}} \frac{\sqrt{s}\, m_T\, e^y - M^2}{\sqrt{s} - m_T\, e^{-y}}. \tag{5}$$

The parton level cross-section $d\sigma/d\hat{t}$ is defined as [8]

$$\frac{d\sigma}{d\hat{t}} = \frac{d\sigma}{d\hat{t}}(ab \to Q\overline{Q}(^{2S+1}L_J) + X)\, M_L(Q\overline{Q}(^{2S+1}L_J) \to \psi). \tag{6}$$

The short distance contribution $d\sigma/d\hat{t}(ab \to Q\overline{Q}(^{2S+1}L_J) + X)$ corresponds to the production of a $Q\bar{Q}$ pair in a particular color and spin configuration can be calculated within the framework of perturbative QCD (pQCD). The long distance matrix elements (LDME) $M_L(Q\overline{Q}(^{2S+1}L_J) \to \psi)$ corresponds to the probability of the $Q\bar{Q}$ state to convert to the quarkonium wavefunction and can be estimated by comparison with experimental measurements. The short distance invariant differential cross-section is given by

$$\frac{d\sigma}{d\hat{t}}(ab \to Q\overline{Q}(^{2S+1}L_J) + X) = \frac{|\mathcal{M}|^2}{16\pi\hat{s}^2}, \tag{7}$$

where $|\mathcal{M}|^2$ is the Feynman squared amplitude. We use the expressions for the short distance CS cross-sections given in Refs. [45–47] and the CO cross-sections given in Refs. [48–50] which we reproduce in the Appendix A. The CTEQ6M [51] parametrization is used for parton distribution functions.

The LDMEs scale with a definite power of the relative velocity v of the heavy quarks inside $Q\bar{Q}$ bound states. In the limit $v \ll 1$, the production of quarkonium is based on the $^3S_1^{[1]}$ and $^3P_J^{[1]}$ ($J = 0,1,2$) CS states and $^1S_0^{[8]}$, $^3S_1^{[8]}$ and $^3P_J^{[8]}$ CO states. The differential cross section for the direct production of J/ψ can be written as the sum of these contributions,

$$\begin{aligned}
d\sigma(J/\psi) = {} & d\sigma(Q\bar{Q}([^3S_1]_1))\, M_L(Q\bar{Q}([^3S_1]_1) \to J/\psi) + d\sigma(Q\bar{Q}([^1S_0]_8))\, M_L(Q\bar{Q}([^1S_0]_8) \to J/\psi) \\
& + d\sigma(Q\bar{Q}([^3S_1]_8))\, M_L(Q\bar{Q}([^3S_1]_8) \to J/\psi) + d\sigma(Q\bar{Q}([^3P_0]_8))\, M_L(Q\bar{Q}([^3P_0]_8) \to J/\psi) \\
& + d\sigma(Q\bar{Q}([^3P_1]_8))\, M_L(Q\bar{Q}([^3P_1]_8) \to J/\psi) + d\sigma(Q\bar{Q}([^3P_2]_8))\, M_L(Q\bar{Q}([^3P_2]_8) \to J/\psi) \\
& + \cdots
\end{aligned} \tag{8}$$

The dots represent contribution of terms at higher powers of v. The contributions from the CO matrix elements in Eq. 8 are suppressed by v^4 compared to the CS matrix elements.

For the case of the p-wave bound states χ_{cJ} (χ_{c0}, χ_{c1} and χ_{c2}), the color-singlet state $Q\bar{Q}[^3P_J]_1$ and the color-octet state $Q\bar{Q}[^3S_1]_8$ contribute to the same order in v (v^5) because

of the angular momentum barrier for the $p-$wave states, and hence both need to be included. The χ_c differential cross section thus can be written as

$$d\sigma(\chi_{cJ}) = d\sigma(Q\bar{Q}([^3P_J]_1))\, M_L(Q\bar{Q}([^3P_J]_1) \to \chi_{cJ}) + d\sigma(Q\bar{Q}([^3S_1]_8))\, M_L(Q\bar{Q}([^3S_1]_8) \to \chi_{cJ})$$

$$+ \cdots$$

$$(9)$$

The prompt J/ψ production at LHC energies consists of direct J/ψ production from the initial parton-parton hard scattering and the feed-down contributions to the J/ψ from the decay of heavier charmonium states $\psi(2S)$, χ_{c0}, χ_{c1} and χ_{c2}. The relevant branching fractions are given in the Table I [52]. The prompt $\psi(2S)$ has no significant feed-down contributions from the higher mass states.

TABLE I. Relevant branching fractions for charmonia [52]

Meson From	to χ_{c0}	to χ_{c1}	to χ_{c2}	to J/ψ
$\psi(2S)$	0.0962	0.092	0.0874	0.595
χ_{c0}				0.0116
χ_{c1}				0.344
χ_{c2}				0.195

The expressions and the values for the color-singlet operators can be found in [48, 49, 53] which are obtained by solving the non-relativistic wavefunctions. The CO operators can not be related to the non-relativistic wavefunctions of $Q\bar{Q}$ since it involves a higher Fock state and thus measured data is used to constrain them. The color-singlet contributions along with their calculated values and color-octet contributions to be fitted are written below for the prompt J/ψ.

1. Direct contributions

$$M_L(c\bar{c}([^3S_1]_1) \to J/\psi) = 1.2\,\text{GeV}^3$$
$$M_L(c\bar{c}([^3S_1]_8) \to J/\psi)$$
$$M_L(c\bar{c}([^1S_0]_8) \to J/\psi)$$
$$M_L(c\bar{c}([^3P_0]_8) \to J/\psi) = \frac{1}{3}M_L(c\bar{c}([^3P_1]_8) \to J/\psi) = \frac{1}{5}M_L(c\bar{c}([^3P_2]_8) \to J/\psi)$$

$$(10)$$

6

2. Feed-down contribution from $\psi(2S)$

$$M_L(c\bar{c}([^3S_1]_1) \to \psi(2S)) = 0.76 \, \text{GeV}^3$$

$$M_L(c\bar{c}([^3S_1]_8) \to \psi(2S))$$

$$M_L(c\bar{c}([^1S_0]_8) \to \psi(2S))$$

$$M_L(c\bar{c}([^3P_0]_8) \to \psi(2S)) = \frac{1}{3}M_L(c\bar{c}([^3P_1]_8) \to \psi(2S)) = \frac{1}{5}M_L(c\bar{c}([^3P_2]_8) \to \psi(2S))$$

$$(11)$$

3. Feed-down contribution from χ_{cJ}

$$M_L(c\bar{c}([^3P_0]_1) \to \chi_{c0}) = 0.054 \, m_c^2 \, \text{GeV}^3$$

$$M_L(c\bar{c}([^3S_1]_8) \to \chi_{c0}) \tag{12}$$

The mass of the charm quark is taken as $m_c = 1.6$ GeV. The short distsnce cross sections $d\sigma(Q\bar{Q}([^1S_0]_8))$ and $d\sigma(Q\bar{Q}([^3P_J]_8))$ have very similar p_T dependence for this reason the transverse momentum distribution is sensitive only to a linear combination of their LDMEs. Following the ref. [48, 54] we fit a linear combination

$$M_L(Q\bar{Q}([^1S_0]_8, [^3P_0]_8) \to \psi) = M_L(Q\bar{Q}([^1S_0]_8) \to \psi) + \frac{k}{m_c^2}M_L(Q\bar{Q}([^3P_0]_8) \to \psi) \tag{13}$$

of these LDMEs. We use $k=3$ for our calculations [48, 54].

III.   RESULTS AND DISCUSSIONS

As discussed in the last section there are two free parameters $(M_L(c\bar{c}([^3S_1]_8 \to J/\psi))$, $M_L(c\bar{c}([^1S_0]_8, [^3P_0]_8) \to J/\psi))$ for J/ψ, two $(M_L(c\bar{c}([^3S_1]_8 \to \psi(2S)))$, $M_L(c\bar{c}([^1S_0]_8, [^3P_0]_8) \to \psi(2S)))$ for $\psi(2S)$ and one $(M_L(c\bar{c}([^3S_1]_8) \to \chi_{c0}))$ for χ_{cJ} to be obtained from the experiments. The measured yields of χ_{cJ} from the following datasets are used to obtain color-octet matrix elements for χ_{cJ}

1. CDF results at $\sqrt{S} = 1.8$ TeV [32].

2. ATLAS results at $\sqrt{S} = 7$ [40].

3. CMS results at $\sqrt{S} = 7$ TeV [38].
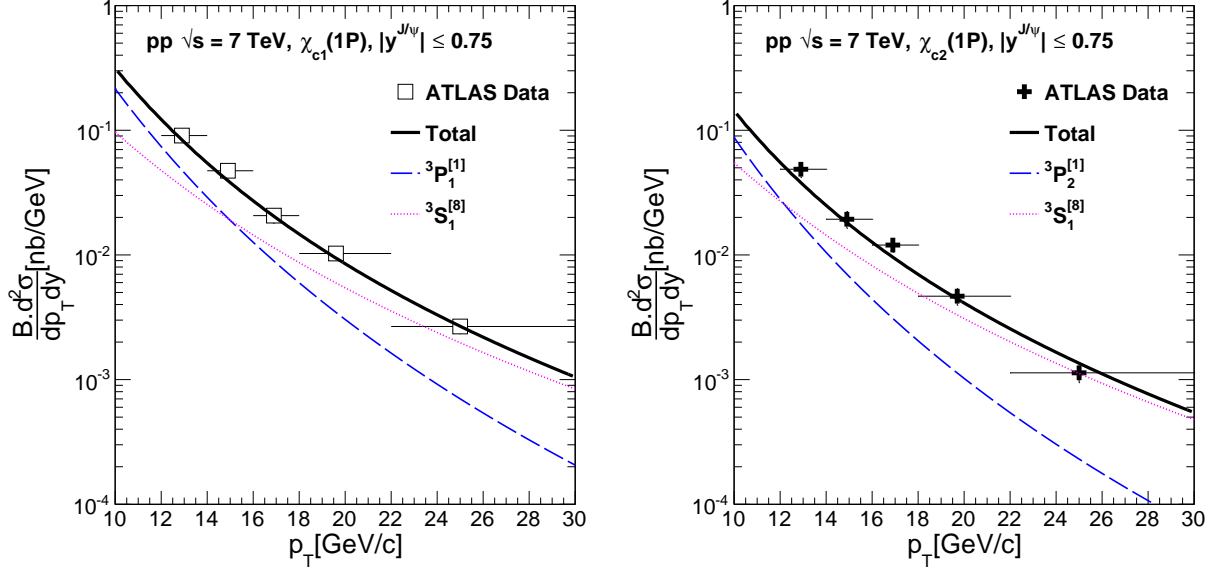
4. LHCb results at $\sqrt{S} = 7$ TeV [44].

FIG. 1. (Color online) The NRQCD calculations of production cross section of χ_{c1} and χ_{c2} in p+p collisions at $\sqrt{s} = 7.0$ TeV as a function of transverse momentum. The Calculations are compared with the measured data by ATLAS experiment at LHC [40]. The χ_c color octet LDMEs are obtained by fitting this data.
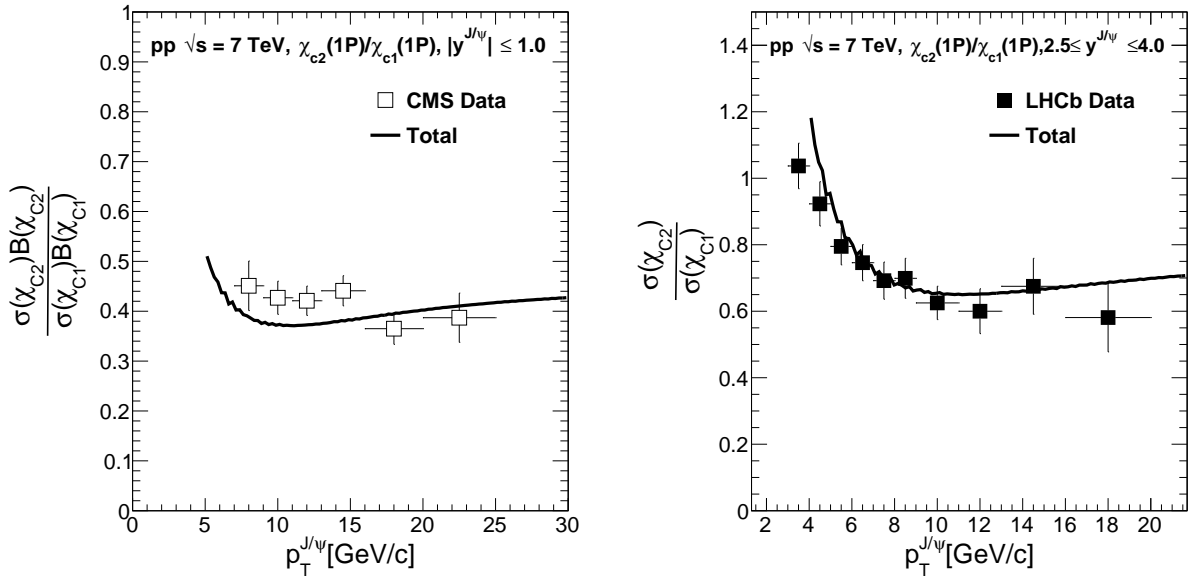

FIG. 2. (Color online) The NRQCD calculations of production cross section ratios of χ_{c2} and χ_{c1} in p+p collisions at $\sqrt{s} = 7.0$ TeV as a function of transverse momentum. The Calculations are compared with the measured data by CMS and LHCb experiments at LHC [38, 44]. The χ_c color octet LDMEs are obtained by fitting this data.
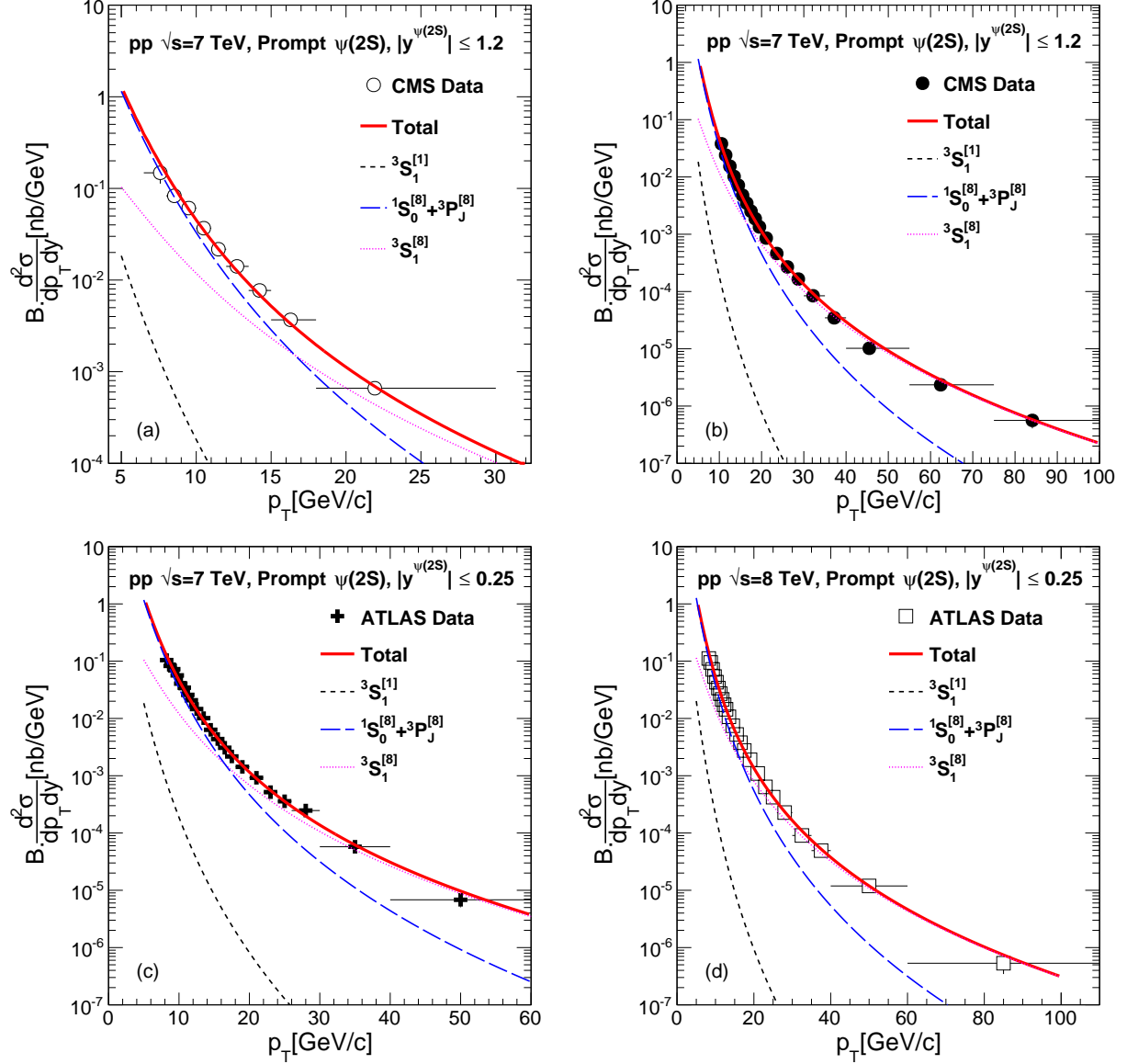
8

FIG. 3. (Color online) The NRQCD calculations of production cross section of $\psi(2S)$ in p+p collisions as a function of transverse momentum compared with the measured data at LHC (a) CMS data at $\sqrt{s} = 7$ TeV [36] (b) CMS data at $\sqrt{s} = 7$ TeV [37] (c) ATLAS data at $\sqrt{s} = 7$ TeV and (d) ATLAS data at $\sqrt{s} = 8$ TeV [39]. The LDMEs are obtained by a combined fit of the LHC and Tevatron data.

Figure 1 shows the NRQCD calculations of production cross section of χ_{c1} and χ_{c2} in p+p collisions at $\sqrt{s} = 7.0$ TeV as a function of transverse momentum. The Calculations are compared with the measured data by ATLAS experiment at LHC [40]. Figure 2 shows the NRQCD calculations of production cross section ratios of χ_{c2} and χ_{c1} in p+p collisions at
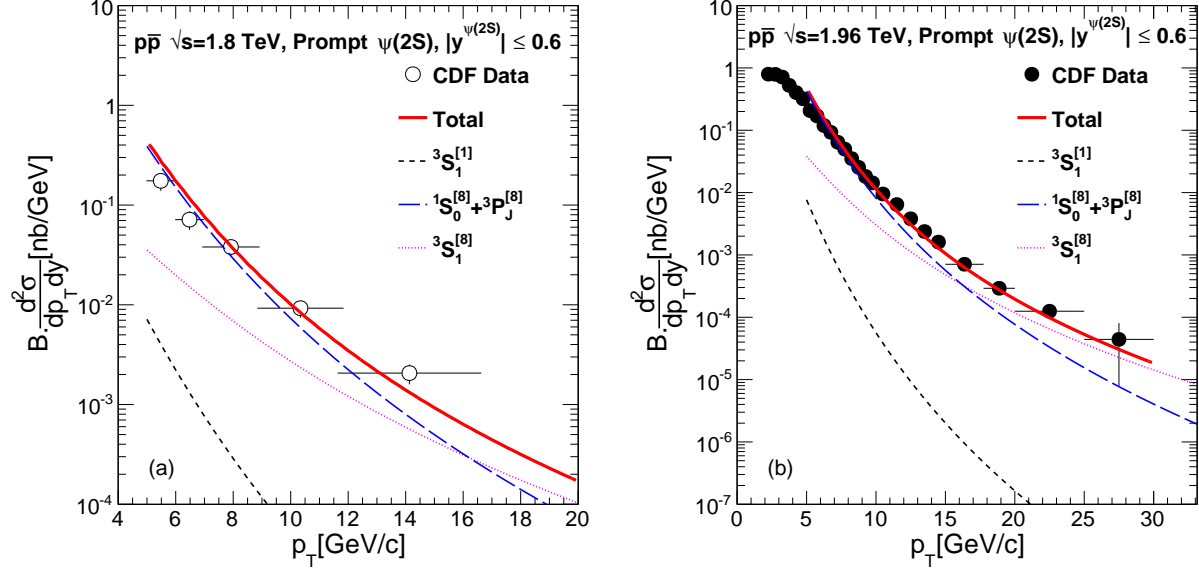
9

FIG. 4. (Color online) The NRQCD calculations of production cross section of $\psi(2S)$ in p+$\bar{\text{p}}$ collisions as a function of transverse momentum compared with the measured data at Tevatron (a) CDF data at $\sqrt{s} = 1.8$ TeV [34] and (b) CDF data at $\sqrt{s} = 1.96$ TeV [35]. The LDMEs are obtained by a combined fit of the Tevatron and LHC data.

$\sqrt{s} = 7.0$ TeV as a function of transverse momentum. The Calculations are compared with the measured data at LHC in panel (a) CMS data at $\sqrt{s} = 7$ TeV [38] and in panel (b) LHCb data at $\sqrt{s} = 7$ TeV [44]. The χ_c color octet LDMEs are obtained by combined fitting of these datasets and its value is

$$M_L(Q\bar{Q}([^3S_1]_8) \to \chi_{c0})/m^2_{\text{charm}} = (0.01112 \pm 0.00068)\,\text{GeV}^3\,, \qquad (14)$$

with a combined $\chi^2/dof = 1.20$.

The measured yields of prompt $\psi(2S)$ from the following datasets are used to obtain color-octet matrix elements for $\psi(2S)$

1. CMS results at $\sqrt{S} = 7$ TeV [36, 37].

2. ATLAS results at $\sqrt{S} = 7$ and 8 TeV [39].

3. CDF results at $\sqrt{S} = 1.8$ TeV [34].

4. CDF results at $\sqrt{S} = 1.96$ TeV [35].

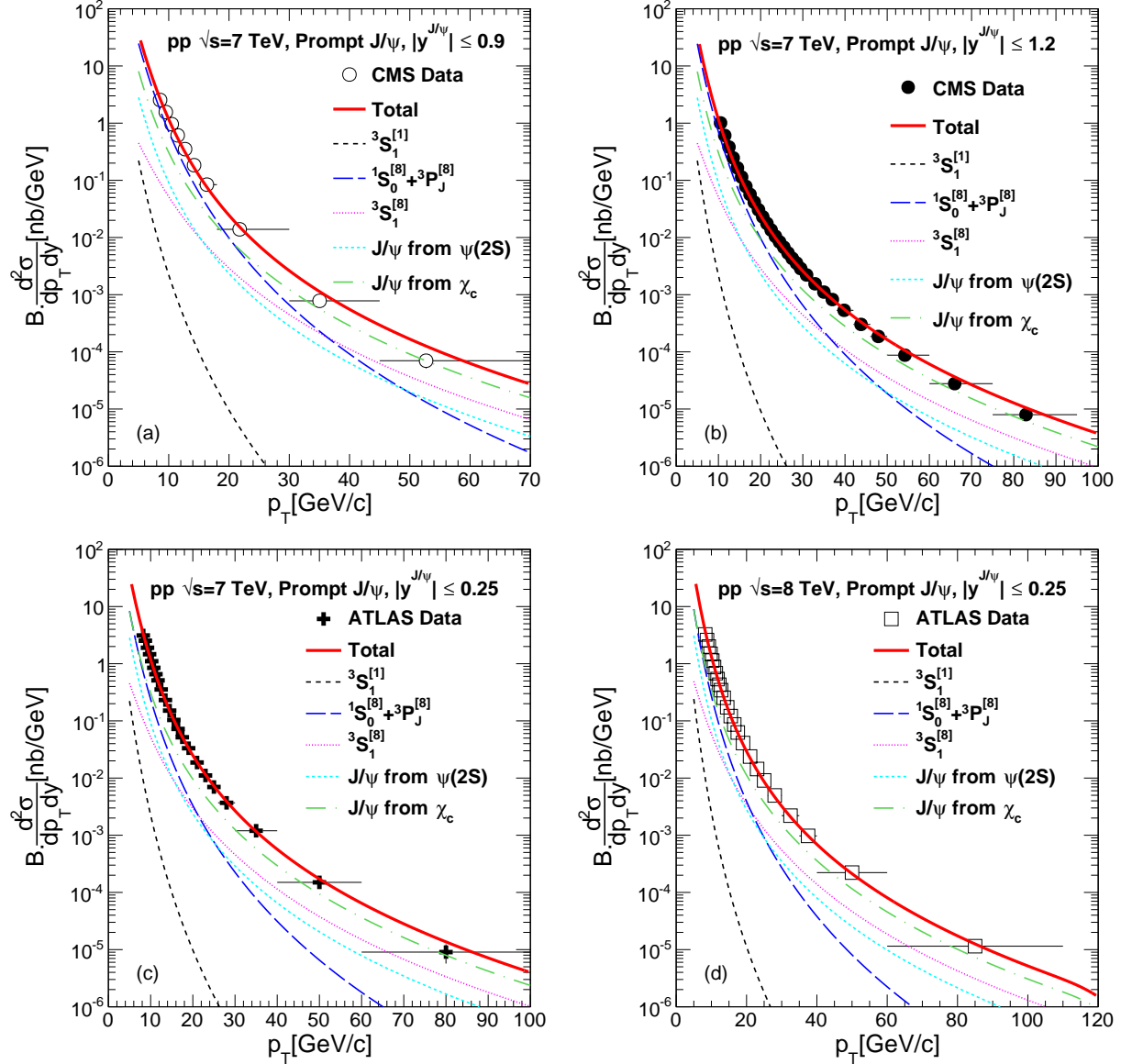5. LHCb results at $\sqrt{S} = 7$ TeV [41].

10

FIG. 5. (Color online) The NRQCD calculations of production cross section of J/ψ in p+p collisions as a function of transverse momentum compared with the measured data at LHC (a) CMS data at $\sqrt{s} = 7$ TeV [36] (b) CMS data at $\sqrt{s} = 7$ TeV [37] (c) ATLAS data at $\sqrt{s} = 7$ TeV and (d) ATLAS data at $\sqrt{s} = 8$ TeV [39]. The LDMEs are obtained by a combined fit of the LHC and Tevatron data.

Figure 3 shows the NRQCD calculations of production cross section of $\psi(2S)$ in p+p collisions as a function of transverse momentum compared with the measured data at LHC in panels (a) CMS data at $\sqrt{s} = 7$ TeV [36], (b) CMS data at $\sqrt{s} = 7$ TeV [37], (c) ATLAS data at $\sqrt{s} = 7$ TeV and, (d) ATLAS data at $\sqrt{s} = 8$ TeV [39]. Figure 4 shows the NRQCD
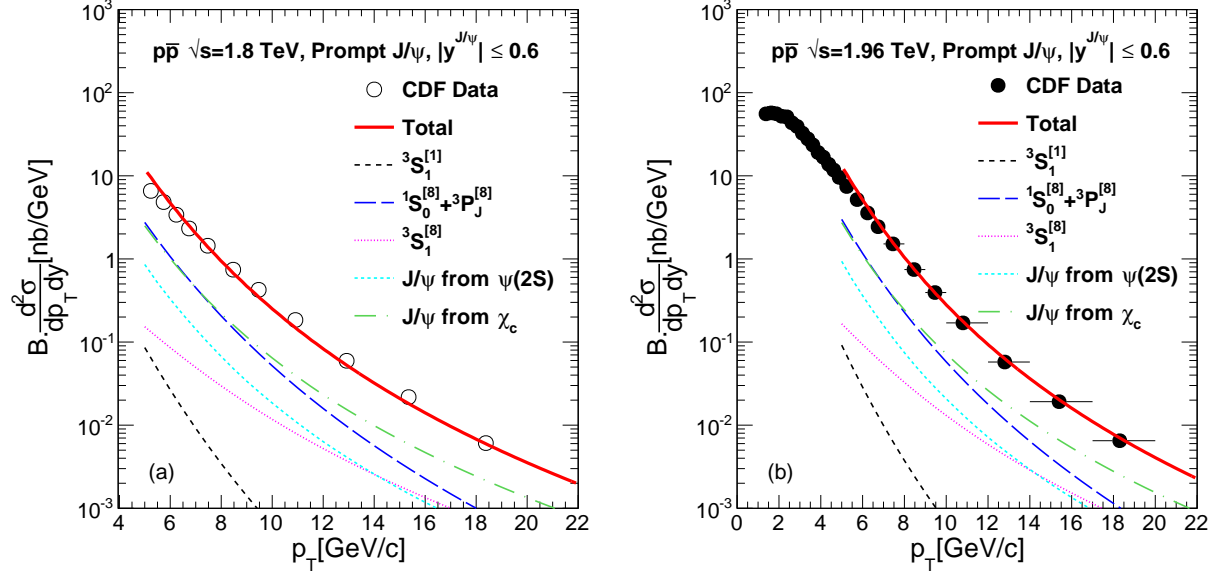
11

FIG. 6. (Color online) The NRQCD calculations of production cross section of J/ψ in p+$\bar{\text{p}}$ collisions as a function of transverse momentum compared with the measured data at Tevatron (a) CDF data at $\sqrt{s} = 1.8$ TeV [34] and (b) CDF data at $\sqrt{s} = 1.96$ TeV [35]. The LDMEs are obtained by a combined fit of the LHC and Tevatron data.

FIG. 7. (Color online) The NRQCD calculations of production cross section of J/ψ in p+p collisions as a function of transverse momentum compared with the measured data at LHC (a) LHCb data at $\sqrt{s} = 7$ TeV [42] and (b) LHCb data at $\sqrt{s} = 13$ TeV [43]. The LDMEs are obtained by a combined fit of the LHC and Tevatron data.
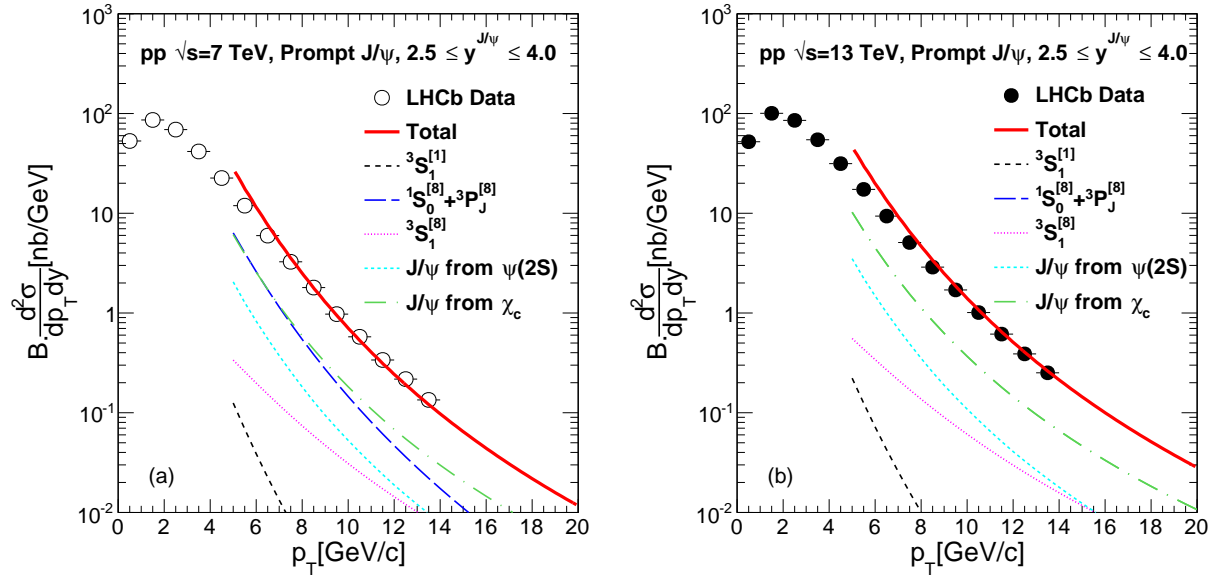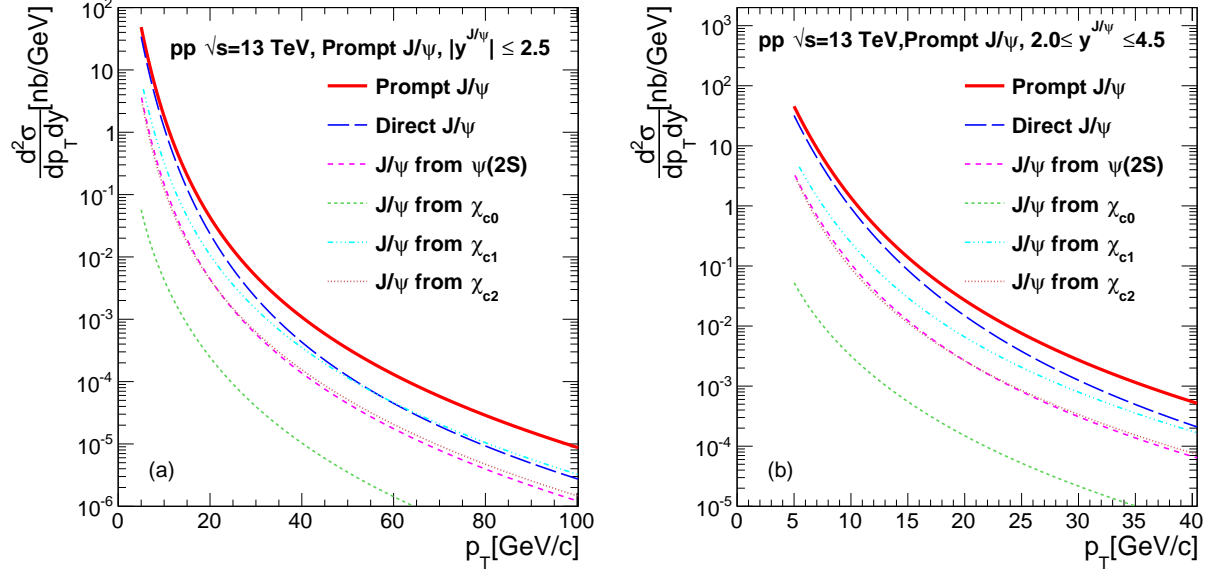
12

FIG. 8. (Color online) The NRQCD calculations of production cross section of J/ψ in p+p collisions as a function of transverse momentum at $\sqrt{s} = 13$ TeV. The calculations are shown in the kinematic bins relevant to (a) CMS, ATLAS and (b) ALICE, LHCb detectors at LHC. For the J/ψ meson all the relevant contributions from higher mass states are also shown.
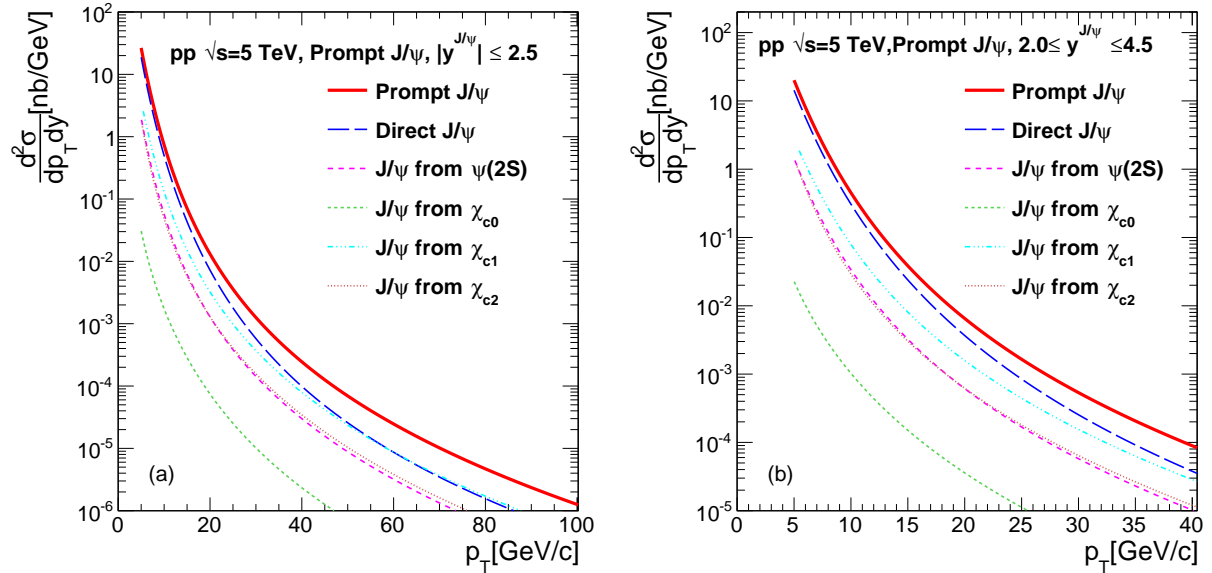

FIG. 9. (Color online)The NRQCD calculations of production cross section of J/ψ in p+p collisions as a function of transverse momentum at $\sqrt{s} = 5$ TeV. The calculations are shown in the kinematic bins relevant to (a) CMS, ATLAS and (b) ALICE, LHCb detectors at LHC. For the J/ψ meson all the relevant contributions from higher mass states are also shown.
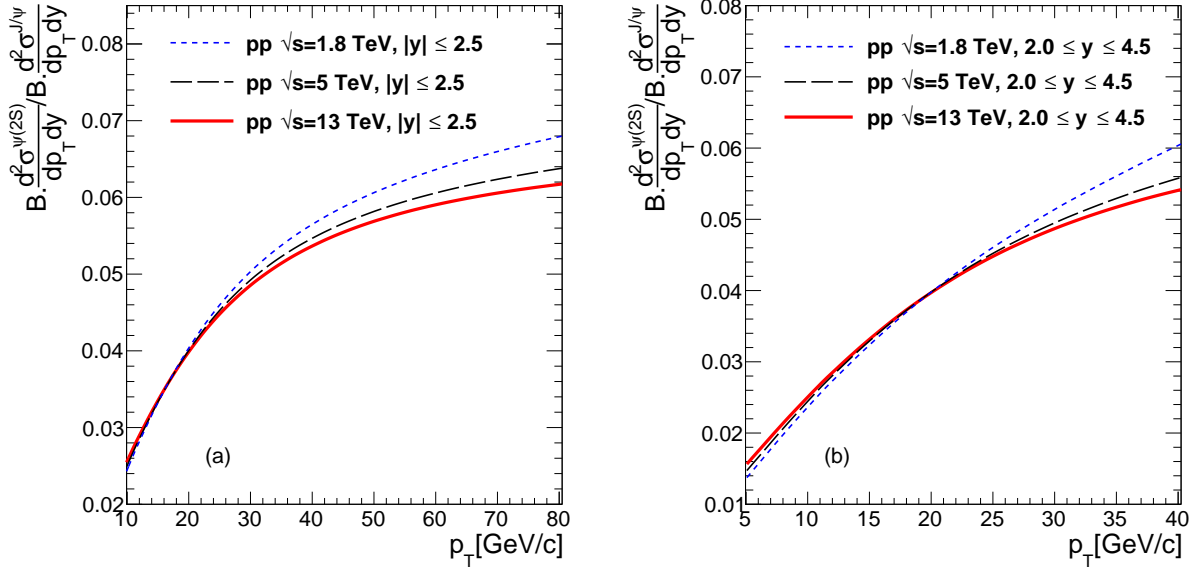
13

FIG. 10. (Color online) The NRQCD calculations of production cross section ratios of $\psi(2S)$ and J/ψ in p+p collisions as a function of transverse momentum at $\sqrt{s} = 1.8$, 5 and 13 TeV. The calculations are shown in the kinematic bins relevant for (a) CMS, ATLAS and (b) ALICE, LHCb detectors at LHC.

calculations of production cross section of $\psi(2S)$ in p+$\bar{\text{p}}$ collisions as a function of transverse momentum compared with the measured data at Tevatron in panels (a) CDF data at $\sqrt{s} = 1.8$ TeV [34] and (b) CDF data at $\sqrt{s} = 1.96$ TeV [35]. We obtain following values of $\psi(2S)$ color-octet matrix elements by a combined fit of the Tevatron and LHC data

$$M_L(c\bar{c}([^3S_1]_8) \to \psi(2S)) = (0.00362 \pm 0.00006 \pm 0.00002)\,\text{GeV}^3$$

$$M_L(Q\bar{Q}([^1S_0]_8, [^3P_0]_8) \to \psi(2S)) = (0.02280 \pm 0.00028 \pm 0.00034)\,\text{GeV}^3 \qquad (15)$$

with a $\chi^2/dof = 2.54$.

Here the first error is due to fitting and the second error is obtained by enhancing the CS cross section 3 times. It is due to the fact that NLO corrections enhance the color-singlet J/ψ production by 2-3 order of magnitude [23]. The NLO corrections to J/ψ production via S-wave color octet (CO) states ($^1S_0^{[8]\,3}S_1^{[8]}$) are found to be small Ref. [24].

To fit the remaining 2 parameters of J/ψ we use the combined fit for the following datasets of prompt J/ψ yields

14

1. CMS results at $\sqrt{S} = 7$ TeV [36, 37].

2. ATLAS results at $\sqrt{S} = 7$ and 8 TeV [39].

3. CDF results at $\sqrt{S} = 1.8$ TeV [34].

4. CDF results at $\sqrt{S} = 1.96$ TeV [35].

5. LHCb results at $\sqrt{S} = 7$ TeV [42].

6. LHCb results at $\sqrt{S} = 13$ TeV [43].

Figures 5 shows the NRQCD calculations of production cross section of J/ψ in p+p collisions as a function of transverse momentum compared with the measured data at LHC in panels (a) CMS data at $\sqrt{s} = 7$ TeV [36] and (b) CMS data at $\sqrt{s} = 7$ TeV [37] (c) ATLAS data at $\sqrt{s} = 7$ TeV and (d) ATLAS data at $\sqrt{s} = 8$ TeV [39]. Figure 6 shows the NRQCD calculations of production cross section of J/ψ in p+$\bar{\text{p}}$ collisions as compared with the measured data at Tevatron in panels (a) CDF data at $\sqrt{s} = 1.8$ TeV [34] and (b) CDF data at $\sqrt{s} = 1.96$ TeV [35]. Figure 7 shows the the NRQCD calculations of production cross section of J/ψ in p+p collisions compared with the forward rapidity data measured at LHC in panels (a) LHCb data at $\sqrt{s} = 7$ TeV [42] and (b) LHCb data at $\sqrt{s} = 13$ TeV [43]. We obtain following values of J/ψ color-octet matrix elements by a combined fit of the Tevatron and the LHC data

$$M_L(c\bar{c}([^3S_1]_8) \to J/\psi) = (0.00206 \pm 0.00014 \pm 0.00001)\, \text{GeV}^3$$

$$M_L(Q\bar{Q}([^1S_0]_8, [^3P_0]_8) \to J/\psi) = (0.06384 \pm 0.00106 \pm 0.00062)\, \text{GeV}^3 \qquad (16)$$

with a $\chi^2/dof = 2.76$.

We use our newly constrained CO LDMEs shown in equation 16 to predict the J/ψ cross-section at 13 TeV and 5 TeV for the kinematical bins relevant to LHC detectors. Figure 8 and Figure 9 shows The NRQCD calculations of production cross section of J/ψ in p+p collisions as a function of transverse momentum at $\sqrt{s} = 13$ TeV and $\sqrt{s} = 5$ TeV. The calculations are shown in the kinematic bins relevant for (a) CMS, ATLAS and (b) ALICE, LHCb detectors at LHC. For the J/ψ meson all the relevant contributions from higher mass states are also shown.

15

Figure. 10 shows the NRQCD calculations of production cross section ratios of $\psi(2S)$ and J/ψ in p+p collisions as a function of transverse momentum at $\sqrt{s} = 1.8$, 5 and 13 TeV. The calculations are shown in the kinematic bins relevant for (a) CMS, ATLAS and (b) ALICE, LHCb detectors at LHC.

IV. SUMMARY

We have presented NRQCD calculations for the differential production cross sections of prompt J/ψ and prompt $\psi(2S)$ in p+p collisions. For the J/ψ meson, all the relevant contributions from higher mass states are estimated. Measured transverse momentum distributions of $\psi(2S)$, χ_c and J/ψ in p +$\bar{\text{p}}$ collisions at $\sqrt{s} = 1.8$, 1.96 TeV and in p+p collisions at 7, 8 and 13 TeV are used to constrain LDMEs. The calculations for prompt J/ψ and prompt $\psi(2S)$ are compared with the measured data at Tevatron and LHC. The formalism provides a very good description of the data in wide energy range. The values of LDMEs are used to predict the charmonia cross sections in p+p collisions at 13 and 5 TeV in kinematic bins relevant for LHC detectors. We also predict the ratios of $\psi(2S)$ and J/ψ for $\sqrt{s} = 1.8$, 5 and 13 TeV.

Appendix A: Short distance pQCD cross sections for quarkonia production

Here we list the lowest order QCD cross sections for the resonance production used in our calculations. We write the formulas in terms of the invariants $\hat{s}$, $\hat{t}$, $\hat{u}$. To order α_s^2 one only has the gluon fusion processes, g g $\to^{(2S+1)} L_J$ which gives resonance with very small p_T, and hence are not used in our calculations. To order α_s^3, on the other hand, one has typically two-by-two scattering processes. The relevant cross sections are given below:

1. Color Singlet PQCD cross sections

- g q $\to {}^{(2S+1)}L_J$ q or (q$\to$ q̄)

$$
\begin{aligned}
\frac{d\sigma}{d\hat{t}}(^1S_0) &= \frac{2\pi\alpha_s{}^3(R_0)^2}{9M\hat{s}^2} \cdot \frac{(\hat{t}-M^2)^2 - 2\hat{s}\hat{u}}{(-\hat{t})(\hat{t}-M^2)^2} \\
\frac{d\sigma}{d\hat{t}}(^3P_0) &= \frac{8\pi\alpha_s{}^3(R_1')^2}{9M^3\hat{s}^2} \cdot \frac{(\hat{t}-3M^2)^2(\hat{s}^2+\hat{u}^2)}{(-\hat{t})(\hat{t}-M^2)^4} \\
\frac{d\sigma}{d\hat{t}}(^3P_1) &= \frac{16\pi\alpha_s{}^3(R_1')^2}{3M^3\hat{s}^2} \cdot \frac{-\hat{t}(\hat{s}^2+\hat{u}^2) - 4M^2\hat{s}\hat{u}}{(\hat{t}-M^2)^4} \\
\frac{d\sigma}{d\hat{t}}(^3P_2) &= \frac{16\pi\alpha_s{}^3(R_1')^2}{9M^3\hat{s}^2} \cdot
\end{aligned}
\tag{A1}
$$
$$
\frac{(\hat{t}-M^2)^2(\hat{t}^2+6M^4) - 2\hat{s}\hat{u}(\hat{t}^2 - 6M^2(\hat{t}-M^2))}{(-\hat{t})(\hat{t}-M^2)^4}
$$

- q q̄ $\to {}^{(2S+1)}L_J$ g

$$
\frac{d\sigma}{d\hat{t}}(^{(2S+1)}L_J) = -\frac{8}{3}\frac{\hat{t}^2}{\hat{s}^2}\frac{d\sigma}{d\hat{t}}(gq \to^{(2S+1)} L_Jq)|_{\hat{t}\leftrightarrow\hat{u}}
\tag{A2}
$$

We define two new variables as a combination of $\hat{s}$, $\hat{t}$ and $\hat{u}$ which can be used to define the g g $\to {}^{(2S+1)}L_J$ g cross sections.

$$
\begin{aligned}
P &= \hat{s}\hat{t} + \hat{t}\hat{u} + \hat{u}\hat{s} \\
Q &= \hat{s}\hat{t}\hat{u}
\end{aligned}
\tag{A3}
$$

$$
\begin{aligned}
\frac{d\sigma}{d\hat{t}}(^1S_0) &= \frac{\pi\alpha_s{}^3(R_0)^2}{M\hat{s}^2}\frac{P^2(M^8 - 2M^4P + P^2 + 2M^2Q)}{Q(Q - M^2P)^2} \\
\frac{d\sigma}{d\hat{t}}(^3S_1) &= \frac{10\pi\alpha_s{}^3(R_0)^2}{9\hat{s}^2}\frac{M(P^2 - M^2Q)}{(Q - M^2P)^2}
\end{aligned}
\tag{A4}
$$

17

$$\frac{d\sigma}{d\hat{t}}(^1P_1) = \frac{40\pi\alpha_s{}^3(R_1')^2}{3M\hat{s}^2} \frac{[-M^{10}P + M^6P^2 + Q(5M^8 - 7M^4P + 2P^2) + 4M^2Q^2]}{(Q - M^2P)^3}$$

$$\frac{d\sigma}{d\hat{t}}(^3P_0) = \frac{4\pi\alpha_s{}^3(R_1')^2}{M^3\hat{s}^2} \frac{1}{Q(Q - M^2P)^4}[9M^4P^4(M^8 - 2M^4P + P^2)$$

$$- 6M^2P^3Q(2M^8 - 5M^4P + P^2)$$

$$- P^2Q^2(M^8 + 2M^4P - P^2)$$

$$+ 2M^2PQ^3(M^4 - P) + 6M^4Q^4]$$

(A5)

$$\frac{d\sigma}{d\hat{t}}(^3P_1) = \frac{12\pi\alpha_s{}^3(R_1')^2}{M^3\hat{s}^2} \frac{P^2\{M^2P^2(M^4 - 4P) - 2Q(M^8 - 5M^4P - P^2) - 15M^2Q^2\}}{(Q - M^2P)^4}$$

$$\frac{d\sigma}{d\hat{t}}(^3P_2) = \frac{4\pi\alpha_s{}^3(R_1')^2}{M^3\hat{s}^2} \frac{1}{Q(Q - M^2P)^4}$$

$$\{12M^4P^4(M^8 - 2M^4P + P^2) - 3M^2P^3Q(8M^8 - M^4P + 4P^2)$$

$$- 2P^2Q^2(7M^8 - 43M^4P - P^2) + M^2PQ^3(16M^4 - 61P)$$

$$+ 12M^4Q^4\}$$

(A6)

2.   Color Octet PQCD cross sections

We list below short distance squared amplitudes for $2 \to 2$ scattering processes which mediate color-octet quarkonia production. These expressions are averaged over initial spins and colors of the two incident partons. The helicity levels of outgoing $J = 1$ and $J = 2$ pairs are labeled by the subscript h.

- $q\,\bar{q} \to Q\bar{Q}[^{(2S+1)}L_J^{(8)}]\,g$

$$\overline{\sum}|\mathcal{A}(q\bar{q} \to Q\overline{Q}[^1S_0^{(8)}]g)|^2 = \frac{5(4\pi\alpha_s)^3}{27M} \frac{\hat{t}^2 + \hat{u}^2}{\hat{s}(\hat{s} - M^2)^2}$$

$$\overline{\sum_{h=0}}|\mathcal{A}(q\bar{q} \to Q\overline{Q}[^3S_1^{(8)}]g)|^2 = \frac{8(4\pi\alpha_s)^3}{81M^3} \frac{M^2\hat{s}}{(\hat{s} - M^2)^4}[4(\hat{t}^2 + \hat{u}^2) - \hat{t}\hat{u}]$$

(A7)

$$\overline{\sum_{|h|=1}}|\mathcal{A}(q\bar{q} \to Q\overline{Q}[^3S_1^{(8)}]g)|^2 = \frac{2(4\pi\alpha_s)^3}{81M^3} \frac{\hat{s}^2 + M^4}{(\hat{s} - M^2)^4} \frac{\hat{t}^2 + \hat{u}^2}{\hat{t}\hat{u}}[4(\hat{t}^2 + \hat{u}^2) - \hat{t}\hat{u}]$$

18

$$\sum |\mathcal{A}(q\bar{q} \to Q\overline{Q}[^3P_0^{(8)}]g)|^2 = \frac{20(4\pi\alpha_s)^3}{81M^3} \frac{(\hat{s}-3M^2)^2(\hat{t}^2+\hat{u}^2)}{\hat{s}(\hat{s}-M^2)^4}$$

$$\sum_{h=0} |\mathcal{A}(q\bar{q} \to Q\overline{Q}[^3P_1^{(8)}]g)|^2 = \frac{40(4\pi\alpha_s)^3}{81M^3} \frac{\hat{s}(\hat{t}^2+\hat{u}^2)}{(\hat{s}-M^2)^4} \qquad \text{(A8)}$$

$$\sum_{|h|=1} |\mathcal{A}(q\bar{q} \to Q\overline{Q}[^3P_1^{(8)}]g)|^2 = \frac{160(4\pi\alpha_s)^3}{81M^3} \frac{M^2\hat{t}\hat{u}}{(\hat{s}-M^2)^4}$$

$$\sum_{h=0} |\mathcal{A}(q\bar{q} \to Q\overline{Q}[^3P_2^{(8)}]g)|^2 = \frac{8(4\pi\alpha_s)^3}{81M^3} \frac{\hat{s}(\hat{t}^2+\hat{u}^2)}{(\hat{s}-M^2)^4}$$

$$\sum_{|h|=1} |\mathcal{A}(q\bar{q} \to Q\overline{Q}[^3P_2^{(8)}]g)|^2 = \frac{32(4\pi\alpha_s)^3}{27M^3} \frac{M^2\hat{t}\hat{u}}{(\hat{s}-M^2)^4} \qquad \text{(A9)}$$

$$\sum_{|h|=2} |\mathcal{A}(q\bar{q} \to Q\overline{Q}[^3P_2^{(8)}]g)|^2 = \frac{16(4\pi\alpha_s)^3}{27M^3} \frac{M^4(\hat{t}^2+\hat{u}^2)}{\hat{s}(\hat{s}-M^2)^4}$$

- $g\,q \to Q\bar{Q}[^{(2S+1)}L_J^{(8)}]\,q$

$$\sum |\mathcal{A}(gq \to Q\overline{Q}[^1S_0^{(8)}]q)|^2 = -\frac{5(4\pi\alpha_s)^3}{72M} \frac{\hat{s}^2+\hat{u}^2}{\hat{t}(\hat{t}-M^2)^2}$$

$$\sum_{h=0} |\mathcal{A}(gq \to Q\overline{Q}[^3S_1^{(8)}]q)|^2 = -\frac{(4\pi\alpha_s)^3}{54M^3} \frac{M^2\hat{t}\big[4(\hat{s}^2+\hat{u}^2)-\hat{s}\hat{u}\big]}{\big[(\hat{s}-M^2)(\hat{t}-M^2)\big]^2}$$

$$\sum_{|h|=1} |\mathcal{A}(gq \to Q\overline{Q}[^3S_1^{(8)}]q)|^2 = -\frac{(4\pi\alpha_s)^3}{108M^3} \qquad \text{(A10)}$$

$$\times \frac{(\hat{s}^2+\hat{u}^2+2M^2\hat{t})(\hat{s}-M^2)^2-2M^2\hat{s}\hat{t}\hat{u}}{\hat{s}\hat{u}\big[(\hat{s}-M^2)(\hat{t}-M^2)\big]^2}$$

$$\times \big[4(\hat{s}^2+\hat{u}^2)-\hat{s}\hat{u}\big]$$

$$\sum |\mathcal{A}(gq \to Q\overline{Q}[^3P_0^{(8)}]q)|^2 = -\frac{5(4\pi\alpha_s)^3}{54M^3} \frac{(\hat{t}-3M^2)^2(\hat{s}^2+\hat{u}^2)}{\hat{t}(\hat{t}-M^2)^4}$$

$$\sum_{h=0} |\mathcal{A}(gq \to Q\overline{Q}[^3P_1^{(8)}]q)|^2 = -\frac{5(4\pi\alpha_s)^3}{27M^3} \frac{\hat{t}\big[\hat{s}^2(\hat{s}-M^2)^2+\hat{u}^2(\hat{s}+M^2)^2\big]}{(\hat{t}-M^2)^4(\hat{s}-M^2)^2} \qquad \text{(A11)}$$

$$\sum_{|h|=1} |\mathcal{A}(gq \to Q\overline{Q}[^3P_1^{(8)}]q)|^2 = -\frac{20(4\pi\alpha_s)^3}{27M^3} \frac{M^2\hat{s}\hat{u}(\hat{t}^2+\hat{t}\hat{u}+\hat{u}^2)}{(\hat{t}-M^2)^4(\hat{s}-M^2)^2}$$

$$\sum_{h=0}^{-} |\mathcal{A}(gq \to Q\overline{Q}[^3P_2^{(8)}]q)|^2 = -\frac{(4\pi\alpha_s)^3}{27M^3}\frac{\hat{t}}{(\hat{t}-M^2)^4}$$

$$\times \left[\hat{s}^2 + \hat{u}^2 + 12M^2\hat{s}\hat{u}^2\frac{\hat{s}^2 + M^2\hat{s} + M^4}{(\hat{s}-M^2)^4}\right]$$

$$\sum_{|h|=1}^{-} |\mathcal{A}(gq \to Q\overline{Q}[^3P_2^{(8)}]q)|^2 = -\frac{4(4\pi\alpha_s)^3}{9M^3}\frac{M^2\hat{s}\hat{u}}{(\hat{t}-M^2)^4}$$

$$\times \frac{(\hat{s}-M^2)^2(\hat{s}^2+M^4)-(\hat{s}+M^2)^2\hat{t}\hat{u}}{(\hat{s}-M^2)^4}$$

(A12)

$$\sum_{|h|=2}^{-} |\mathcal{A}(gq \to Q\overline{Q}[^3P_2^{(8)}]q)|^2 = -\frac{2(4\pi\alpha_s)^3}{9M^3}\frac{M^4}{\hat{t}(\hat{t}-M^2)^4}$$

$$\times \left[\hat{s}^2 + \hat{u}^2 + 2\hat{s}^2\hat{t}\hat{u}\frac{(\hat{s}-M^2)(2\hat{t}+\hat{u})-\hat{u}^2}{(\hat{s}-M^2)^4}\right]$$

- g g $\to Q\bar{Q}[^{(2S+1)}L_J^{(8)}]$ g (The $gg \to Q\overline{Q}[^3P_J^{(8)}]$ g squared amplitudes are expressed in terms of the variables $\hat{s}$ and $\hat{z} \equiv \sqrt{\hat{t}\hat{u}}$.)

$$\sum^{-} |\mathcal{A}(gg \to Q\overline{Q}[^1S_0^{(8)}]g)|^2 = \frac{5(4\pi\alpha_s)^3}{16M}\left[\hat{s}^2(\hat{s}-M^2)^2 + \hat{s}\hat{t}\hat{u}(M^2-2\hat{s}) + (\hat{t}\hat{u})^2\right]$$

$$\times \frac{(\hat{s}^2 - M^2\hat{s} + M^4)^2 - \hat{t}\hat{u}(2\hat{t}^2 + 3\hat{t}\hat{u} + 2\hat{u}^2)}{\hat{s}\hat{t}\hat{u}\left[(\hat{s}-M^2)(\hat{t}-M^2)(\hat{u}-M^2)\right]^2}$$

$$\sum_{h=0}^{-} |\mathcal{A}(gg \to Q\overline{Q}[^3S_1^{(8)}]g)|^2 = -\frac{(4\pi\alpha_s)^3}{144M^3}\frac{2M^2\hat{s}}{(\hat{s}-M^2)^2}(\hat{t}^2+\hat{u}^2)\hat{t}\hat{u}$$

(A13)

$$\times \frac{27(\hat{s}\hat{t} + \hat{t}\hat{u} + \hat{u}\hat{s}) - 19M^4}{\left[(\hat{s}-M^2)(\hat{t}-M^2)(\hat{u}-M^2)\right]^2}$$

$$\sum_{|h|=1}^{-} |\mathcal{A}(gg \to Q\overline{Q}[^3S_1^{(8)}]g)|^2 = -\frac{(4\pi\alpha_s)^3}{144M^3}\frac{\hat{s}^2}{(\hat{s}-M^2)^2}$$

$$\times \left[(\hat{s}-M^2)^4 + \hat{t}^4 + \hat{u}^4 + 2M^4\left(\frac{\hat{t}\hat{u}}{\hat{s}}\right)^2\right]$$

(A14)

$$\times \frac{27(\hat{s}\hat{t} + \hat{t}\hat{u} + \hat{u}\hat{s}) - 19M^4}{\left[(\hat{s}-M^2)(\hat{t}-M^2)(\hat{u}-M^2)\right]^2}$$

$$\sum \overline{} |\mathcal{A}(gg \to Q\overline{Q}[^3P_0^{(8)}]g)|^2 = \frac{5(4\pi\alpha_s)^3}{12M^3} \frac{1}{\left[\hat{s}\hat{z}^2(\hat{s}-M^2)^4(\hat{s}M^2+\hat{z}^2)^4\right]}$$

$$\times \Big\{ \hat{s}^2\hat{z}^4(\hat{s}^2-\hat{z}^2)^4 + M^2\hat{s}\hat{z}^2(\hat{s}^2-\hat{z}^2)^2(3\hat{s}^2-2\hat{z}^2)(2\hat{s}^4-6\hat{s}^2\hat{z}^2+3\hat{z}^4)$$

$$+ M^4\big[9\hat{s}^{12} - 84\hat{s}^{10}\hat{z}^2 + 265\hat{s}^8\hat{z}^4 - 382\hat{s}^6\hat{z}^6 + 276\hat{s}^4\hat{z}^8 - 88\hat{s}^2\hat{z}^{10} + 9\hat{z}^{12}\big]$$

$$- M^6\hat{s}\big[54\hat{s}^{10} - 357\hat{s}^8\hat{z}^2 + 844\hat{s}^6\hat{z}^4 - 898\hat{s}^4\hat{z}^6 + 439\hat{s}^2\hat{z}^8 - 81\hat{z}^{10}\big]$$

$$+ M^8\big[153\hat{s}^{10} - 798\hat{s}^8\hat{z}^2 + 1415\hat{s}^6\hat{z}^4 - 1041\hat{s}^4\hat{z}^6 + 301\hat{s}^2\hat{z}^8 - 18\hat{z}^{10}\big]$$

$$- M^{10}\hat{s}\big[270\hat{s}^8 - 1089\hat{s}^6\hat{z}^2 + 1365\hat{s}^4\hat{z}^4 - 616\hat{s}^2\hat{z}^6 + 87\hat{z}^8\big]$$

$$+ M^{12}\big[324\hat{s}^8 - 951\hat{s}^6\hat{z}^2 + 769\hat{s}^4\hat{z}^4 - 189\hat{s}^2\hat{z}^6 + 9\hat{z}^8\big]$$

$$- 9M^{14}\hat{s}\big[(6\hat{s}^2 - \hat{z}^2)(5\hat{s}^4 - 9\hat{s}^2\hat{z}^2 + 3\hat{z}^4)\big]$$

$$+ 3M^{16}\hat{s}^2\big[51\hat{s}^4 - 59\hat{s}^2\hat{z}^2 + 12\hat{z}^4\big]$$

$$- 27M^{18}\hat{s}^3\big[2\hat{s}^2 - \hat{z}^2\big]$$

$$+ 9M^{20}\hat{s}^4 \Big\}$$

$$(A15)$$

$$\sum_{h=0} \overline{} |\mathcal{A}(gg \to Q\overline{Q}[^3P_1^{(8)}]g)|^2 = \frac{5(4\pi\alpha_s)^3}{6M^3} \frac{1}{\left[(\hat{s}-M^2)^4(\hat{s}M^2+\hat{z}^2)^4\right]}$$

$$\times \hat{s}\hat{z}^2\big[(\hat{s}^2-\hat{z}^2)^2 - 2M^2\hat{s}\hat{z}^2 - M^4(\hat{s}^2+2\hat{z}^2) + M^8\big] \quad (A16)$$

$$\times \big[(\hat{s}^2-\hat{z}^2)^2 - M^2\hat{s}(2\hat{s}^2-\hat{z}^2) + M^4\hat{s}^2\big]$$

$$\sum_{|h|=1} \overline{} |\mathcal{A}(gg \to Q\overline{Q}[^3P_1^{(8)}]g)|^2 = \frac{5(4\pi\alpha_s)^3}{6M^3} \frac{1}{\left[(\hat{s}-M^2)^4(\hat{s}M^2+\hat{z}^2)^4\right]}$$

$$\times M^2\Big\{ 2(\hat{s}^2-\hat{z}^2)^2(\hat{s}^6 - 4\hat{s}^4\hat{z}^2 + \hat{s}^2\hat{z}^4 - \hat{z}^6)$$

$$- M^2\hat{s}(2\hat{s}^2-\hat{z}^2)(5\hat{s}^6 - 17\hat{s}^4\hat{z}^2 + 9\hat{s}^2\hat{z}^4 - \hat{z}^6)$$

$$+ M^4(21\hat{s}^8 - 49\hat{s}^6\hat{z}^2 + 21\hat{s}^4\hat{z}^4 - 4\hat{s}^2\hat{z}^6 + \hat{z}^8) \quad (A17)$$

$$- M^6\hat{s}(24\hat{s}^6 - 30\hat{s}^4\hat{z}^2 + 6\hat{s}^2\hat{z}^4 - \hat{z}^6)$$

$$+ M^8\hat{s}^2(16\hat{s}^4 - 9\hat{s}^2\hat{z}^2 + 2\hat{z}^4)$$

$$- M^{10}\hat{s}^3(6\hat{s}^2 - \hat{z}^2)$$

$$+ M^{12}\hat{s}^4 \Big\}$$

$$\overline{\sum_{h=0}} |\mathcal{A}(gg \to Q\overline{Q}[^3P_2^{(8)}]g)|^2 = \frac{(4\pi\alpha_s)^3}{6M^3} \frac{\hat{s}\hat{z}^2}{\left[(\hat{s} - M^2)^6(\hat{s}M^2 + \hat{z}^2)^4\right]}$$

$$\left\{\hat{s}^2(\hat{s}^2 - \hat{z}^2)^4 - M^2\hat{s}\hat{z}^2(\hat{s}^2 - \hat{z}^2)^2(11\hat{s}^2 + 2\hat{z}^2)\right.$$

$$+ M^4\left[\hat{s}^8 - 12\hat{s}^6\hat{z}^2 + 41\hat{s}^4\hat{z}^4 - 20\hat{s}^2\hat{z}^6 + \hat{z}^8\right]$$

$$- M^6\hat{s}\left[4\hat{s}^6 - 26\hat{s}^4\hat{z}^2 - \hat{s}^2\hat{z}^4 - 5\hat{z}^6\right]$$

$$+ M^8\left[29\hat{s}^6 - 114\hat{s}^4\hat{z}^2 + 108\hat{s}^2\hat{z}^4 - 10\hat{z}^6\right] \qquad \text{(A18)}$$

$$- M^{10}\hat{s}\left[65\hat{s}^4 - 104\hat{s}^2\hat{z}^2 - 33\hat{z}^4\right]$$

$$+ M^{12}\left[54\hat{s}^4 - 20\hat{s}^2\hat{z}^2 + 7\hat{z}^4\right]$$

$$- M^{14}\hat{s}\left[23\hat{s}^2 + 5\hat{z}^2\right]$$

$$\left. + 7M^{16}\hat{s}^2\right\}$$

$$\overline{\sum_{|h|=1}} |\mathcal{A}(gg \to Q\overline{Q}[^3P_2^{(8)}]g)|^2 = \frac{(4\pi\alpha_s)^3}{2M^3} \frac{M^2}{\left[(\hat{s} - M^2)^6(\hat{s}M^2 + \hat{z}^2)^4\right]}$$

$$\times \left\{2\hat{s}^2(\hat{s}^2 - \hat{z}^2)^2(\hat{s}^6 - 4\hat{s}^4\hat{z}^2 + \hat{s}^2\hat{z}^4 - \hat{z}^6)\right.$$

$$- M^2\hat{s}\left[10\hat{s}^{10} - 37\hat{s}^8\hat{z}^2 + 19\hat{s}^6\hat{z}^4 + 11\hat{s}^4\hat{z}^6 - \hat{s}^2\hat{z}^8 - 4\hat{z}^{10}\right]$$

$$+ M^4\left[25\hat{s}^{10} - 61\hat{s}^8\hat{z}^2 + 27\hat{s}^6\hat{z}^4 - 34\hat{s}^4\hat{z}^6 + 23\hat{s}^2\hat{z}^8 - 2\hat{z}^{10}\right]$$

$$- M^6\hat{s}\left[42\hat{s}^8 - 77\hat{s}^6\hat{z}^2 + 41\hat{s}^4\hat{z}^4 - 22\hat{s}^2\hat{z}^6 + 17\hat{z}^8\right]$$

$$+ M^8\left[53\hat{s}^8 - 88\hat{s}^6\hat{z}^2 + 69\hat{s}^4\hat{z}^4 - 68\hat{s}^2\hat{z}^6 + 3\hat{z}^8\right]$$

$$- M^{10}\hat{s}\left[54\hat{s}^6 - 85\hat{s}^4\hat{z}^2 + 60\hat{s}^2\hat{z}^4 - 9\hat{z}^6\right]$$

$$+ M^{12}\hat{s}^2\left[43\hat{s}^4 - 47\hat{s}^2\hat{z}^2 + 20\hat{z}^4\right]$$

$$- M^{14}\hat{s}^3\left[22\hat{s}^2 - 9\hat{z}^2\right]$$

$$\left. + 5M^{16}\hat{s}^4\right\}$$

$$\text{(A19)}$$

$$\sum_{|h|=2} \overline{|\mathcal{A}(gg \to Q\overline{Q}[^3P_2^{(8)}]g)|^2} = \frac{(4\pi\alpha_s)^3}{2M^3} \frac{M^4}{\left[\hat{s}\hat{z}^2(\hat{s}-M^2)^6(\hat{s}M^2+\hat{z}^2)^4\right]}$$

$$\times \Bigg\{ 2\hat{s}^2\Big[\hat{s}^{12} - 8\hat{s}^{10}\hat{z}^2 + 22\hat{s}^8\hat{z}^4 - 24\hat{s}^6\hat{z}^6 + 10\hat{s}^4\hat{z}^8 - 3\hat{s}^2\hat{z}^{10} + \hat{z}^{12}\Big]$$

$$- M^2\hat{s}\Big[16\hat{s}^{12} - 102\hat{s}^{10}\hat{z}^2 + 210\hat{s}^8\hat{z}^4 - 153\hat{s}^6\hat{z}^6 + 36\hat{s}^4\hat{z}^8 - 6\hat{s}^2\hat{z}^{10} + 4\hat{z}^{12}\Big]$$

$$+ M^4\Big[60\hat{s}^{12} - 306\hat{s}^{10}\hat{z}^2 + 482\hat{s}^8\hat{z}^4 - 271\hat{s}^6\hat{z}^6 + 77\hat{s}^4\hat{z}^8 - 18\hat{s}^2\hat{z}^{10} + 2\hat{z}^{12}\Big]$$

$$- M^6\hat{s}\Big[140\hat{s}^{10} - 573\hat{s}^8\hat{z}^2 + 710\hat{s}^6\hat{z}^4 - 344\hat{s}^4\hat{z}^6 + 91\hat{s}^2\hat{z}^8 - 18\hat{z}^{10}\Big]$$

$$+ M^8\Big[226\hat{s}^{10} - 741\hat{s}^8\hat{z}^2 + 737\hat{s}^6\hat{z}^4 - 310\hat{s}^4\hat{z}^6 + 77\hat{s}^2\hat{z}^8 - 4\hat{z}^{10}\Big]$$

$$- M^{10}\hat{s}\Big[264\hat{s}^8 - 686\hat{s}^6\hat{z}^2 + 541\hat{s}^4\hat{z}^4 - 177\hat{s}^2\hat{z}^6 + 25\hat{z}^8\Big]$$

$$+ M^{12}\Big[226\hat{s}^8 - 452\hat{s}^6\hat{z}^2 + 261\hat{s}^4\hat{z}^4 - 55\hat{s}^2\hat{z}^6 + 2\hat{z}^8\Big]$$

$$- M^{14}\hat{s}\Big[140\hat{s}^6 - 201\hat{s}^4\hat{z}^2 + 71\hat{s}^2\hat{z}^4 - 6\hat{z}^6\Big]$$

$$+ M^{16}\hat{s}^2\Big[60\hat{s}^4 - 53\hat{s}^2\hat{z}^2 + 8\hat{z}^4\Big]$$

$$- 2M^{18}\hat{s}^3\Big[8\hat{s}^2 - 3\hat{z}^2\Big]$$

$$+ 2M^{20}\hat{s}^4 \Bigg\}$$

$$\text{(A20)}$$

[1] J. E. Augustin *et al.* [SLAC-SP-017 Collaboration], "Discovery of a Narrow Resonance in e+ e- Annihilation," Phys. Rev. Lett. **33**, 1406 (1974) [Adv. Exp. Phys. **5**, 141 (1976)].

[2] J. J. Aubert *et al.* [E598 Collaboration], "Experimental Observation of a Heavy Particle J," Phys. Rev. Lett. **33**, 1404 (1974).

[3] V. Kumar, P. Shukla and R. Vogt, "Quarkonia suppression in PbPb collisions at $\sqrt{s_{NN}} = 2.76$ TeV," Phys. Rev. C **92**, 024908 (2015).

[4] S. Chatrchyan *et al.* [CMS Collaboration], "Observation of sequential Upsilon suppression in PbPb collisions," Phys. Rev. Lett. **109**, 222301 (2012).

[5] V. Khachatryan *et al.* [CMS Collaboration], "Measurement of Prompt $\psi(2S) \to J/\psi$ Yield Ratios in Pb-Pb and $p-p$ Collisions at $\sqrt{s_{NN}} = 2.76\text{TeV}$," Phys. Rev. Lett. **113**, no. 26, 262301 (2014).

[6] P. Nason, S. Dawson and R. K. Ellis, "The Total Cross-Section For The Production Of Heavy Quarks In Hadronic Collisions," Nucl. Phys. B **303**, 607 (1988).

[7] P. Nason, S. Dawson and R. K. Ellis, "The One Particle Inclusive Differential Cross-Section For Heavy Quark Production In Hadronic Collisions," Nucl. Phys. B **327**, 49 (1989). [Erratum-ibid. B **335**, 260 (1990)].

[8] G. T. Bodwin, E. Braaten, and G. P. Lepage, "Rigorous QCD analysis of inclusive annihilation and production of heavy quarkonium," Phys. Rev. D **51** 1125 (1995), [Erratum-ibid. D **55** 5853 (1997)].

[9] N. Brambilla *et al.*, "Heavy quarkonium: progress, puzzles, and opportunities," Eur. Phys. J. C **71**, 1534 (2011).

[10] N. Brambilla *et al.*, "QCD and Strongly Coupled Gauge Theories: Challenges and Perspectives," Eur. Phys. J. C **74**, no. 10, 2981 (2014).

[11] M. B. Einhorn and S. D. Ellis, "Hadronic Production Of The New Resonances: Probing Gluon Distributions," Phys. Rev. D **12** 2007 (1975).

[12] S. D. Ellis, M. B. Einhorn, and C. Quigg, "Comment On Hadronic Production Of Psions," Phys. Rev. Lett. **36** 1263 (1976).

[13] C. E. Carlson and R. Suaya, "Hadronic Production Of Psi/J Mesons," Phys. Rev. D **14** 3115 (1976).

[14] E. L. Berger and D. L. Jones, "Inelastic Photoproduction of J/psi and Upsilon by Gluons," Phys. Rev. D **23**, 1521 (1981).

[15] G. A. Schuler, "Quarkonium production and decays," [arXiv:hep-ph/9403387].

[16] P. Artoisenet, J. P. Lansberg, and F. Maltoni, "Hadroproduction of J/ψ and v in association with a heavy-quark pair," Phys. Lett. B **653** 60 (2007).

[17] J. M. Campbell, F. Maltoni, and F. Tramontano, "QCD corrections to J/psi and Upsilon production at hadron colliders," Phys. Rev. Lett. **98** 252002 (2007).

[18] P. Artoisenet, J. M. Campbell, J. P. Lansberg, F. Maltoni, and F. Tramontano, "Υ Production at Fermilab Tevatron and LHC Energies," Phys. Rev. Lett. **101** 152001 (2008).

[19] H. Fritzsch, "Producing Heavy Quark Flavors in Hadronic Collisions: A Test of Quantum Chromodynamics," Phys. Lett. B **67**, 217 (1977).

[20] J. F. Amundson, O. J. P. Eboli, E. M. Gregores and F. Halzen, "Colorless states in perturbative QCD: Charmonium and rapidity gaps," Phys. Lett. B **372**, 127 (1996).

[21] J. F. Amundson, O. J. P. Eboli, E. M. Gregores and F. Halzen, "Quantitative tests of color evaporation: Charmonium production," Phys. Lett. B **390**, 323 (1997).

[22] R. Sharma and I. Vitev, "High transverse momentum quarkonium production and dissociation in heavy ion collisions," Phys. Rev. C **87**, no. 4, 044905 (2013).

[23] B. Gong and J. X. Wang, "Next-to-leading-order QCD corrections to J/ψ polarization at Tevatron and Large-Hadron-Collider energies," Phys. Rev. Lett. **100**, 232001 (2008).

[24] B. Gong, X. Q. Li and J. X. Wang, "QCD corrections to J/ψ production via color octet states at Tevatron and LHC," Phys. Lett. B **673**, 197 (2009), [Phys. Lett. **693**, 612 (2010)].

[25] Y. Q. Ma, K. Wang and K. T. Chao, "QCD radiative corrections to χ_{cJ} production at hadron colliders," Phys. Rev. D **83**, 111503 (2011).

[26] M. Butenschoen and B. A. Kniehl, "J/psi polarization at Tevatron and LHC: Nonrelativistic-QCD factorization at the crossroads," Phys. Rev. Lett. **108**, 172002 (2012).

[27] K. T. Chao, Y. Q. Ma, H. S. Shao, K. Wang and Y. J. Zhang, "J/ψ Polarization at Hadron Colliders in Nonrelativistic QCD," Phys. Rev. Lett. **108**, 242004 (2012).

[28] B. Gong, L. P. Wan, J. X. Wang and H. F. Zhang, "Polarization for Prompt J/ψ and $\psi(2S)$ Production at the Tevatron and LHC," Phys. Rev. Lett. **110**, 042002 (2013).

[29] M. Butenschoen and B. A. Kniehl, "Reconciling J/ψ production at HERA, RHIC, Tevatron, and LHC with NRQCD factorization at next-to-leading order," Phys. Rev. Lett. **106**, 022003 (2011).

[30] Y. Q. Ma, K. Wang and K. T. Chao, "A complete NLO calculation of the J/ψ and ψ' production at hadron colliders," Phys. Rev. D **84**, 114001 (2011), [arXiv:1012.1030 [hep-ph]].

[31] H. S. Shao, H. Han, Y. Q. Ma, C. Meng, Y. J. Zhang and K. T. Chao, "Yields and polarizations of prompt J/ψ and $\psi(2S)$ production in hadronic collisions," JHEP **1505**, 103 (2015).

[32] F. Abe *et al.* [CDF Collaboration], "Production of J/ψ mesons from χ_c meson decays in $p\bar{p}$ collisions at $\sqrt{s} = 1.8$ TeV," Phys. Rev. Lett. **79**, 578 (1997).

[33] A. Abulencia *et al.* [CDF Collaboration], "Measurement of $\sigma_{\chi_{c2}}\mathcal{B}(\chi_{c2} \to J/\psi\gamma)/\sigma_{\chi_{c1}}\mathcal{B}(\chi_{c1} \to J/\psi\gamma)$ in $p\bar{p}$ collisions at $\sqrt{s} = 1.96$-TeV," Phys. Rev. Lett. **98**, 232001 (2007),[hep-ex/0703028 [HEP-EX]].

[34] F. Abe *et al.* [CDF Collaboration], "J/ψ and $\psi(2S)$ production in $p\bar{p}$ collisions at $\sqrt{s} = 1.8$ TeV," Phys. Rev. Lett. **79**, 572 (1997).

[35] D. Acosta *et al.* [CDF Collaboration], "Measurement of the J/ψ meson and $b-$hadron production cross sections in $p\bar{p}$ collisions at $\sqrt{s} = 1960$ GeV," Phys. Rev. D **71**, 032001 (2005).

[36] S. Chatrchyan *et al.* [CMS Collaboration], "J/ψ and ψ_{2S} production in pp collisions at $\sqrt{s} = 7$ TeV," JHEP **1202**, 011 (2012).

[37] V. Khachatryan *et al.* [CMS Collaboration], "Measurement of J/ψ and $\psi(2S)$ Prompt Double-Differential Cross Sections in pp Collisions at $\sqrt{s}$=7TeV," Phys. Rev. Lett. **114**, no. 19, 191802 (2015).

[38] S. Chatrchyan *et al.* [CMS Collaboration], "Measurement of the relative prompt production rate of χ_{c2} and χ_{c1} in pp collisions at $\sqrt{s} = 7$ TeV," Eur. Phys. J. C **72**, 2251 (2012),[arXiv:1210.0875 [hep-ex]].

[39] G. Aad *et al.* [ATLAS Collaboration], "Measurement of the differential cross-sections of prompt and non-prompt production of J/ψ and $\psi(2S)$ in pp collisions at $\sqrt{s} = 7$ and 8 TeV with the ATLAS detector," arXiv:1512.03657 [hep-ex].

[40] G. Aad *et al.* [ATLAS Collaboration], "Measurement of χ_{c1} and χ_{c2} production with $\sqrt{s} = 7$ TeV pp collisions at ATLAS," JHEP **1407**, 154 (2014), [arXiv:1404.7035 [hep-ex]].

[41] R. Aaij *et al.* [LHCb Collaboration], "Measurement of $\psi(2S)$ meson production in pp collisions at $\sqrt{s}$=7 TeV," Eur. Phys. J. C **72**, 2100 (2012).

[42] R. Aaij *et al.* [LHCb Collaboration], "Measurement of J/ψ production in pp collisions at $\sqrt{s} = 7$ TeV," Eur. Phys. J. C **71**, 1645 (2011).

[43] R. Aaij *et al.* [LHCb Collaboration], "Measurement of forward J/ψ production cross-sections in pp collisions at $\sqrt{s} = 13$ TeV," JHEP **1510**, 172 (2015).

[44] R. Aaij *et al.* [LHCb Collaboration], "Measurement of the relative rate of prompt χ_{c0}, χ_{c1} and χ_{c2} production at $\sqrt{s} = 7$TeV," JHEP **1310**, 115 (2013), [arXiv:1307.4285 [hep-ex]].

[45] R. Baier and R. Ruckl, "Hadronic Collisions: A Quarkonium Factory," Z. Phys. C **19**, 251 (1983).

[46] B. Humpert, "Narrow Heavy Resonance Production By Gluons," Phys. Lett. B **184**, 105 (1987).

[47] R. Gastmans, W. Troost and T. T. Wu, "Production of Heavy Quarkonia From Gluons," Nucl. Phys. B **291**, 731 (1987).

[48] P. L. Cho and A. K. Leibovich, "Color octet quarkonia production," Phys. Rev. D **53**, 150 (1996).

[49] P. L. Cho and A. K. Leibovich, "Color octet quarkonia production. 2.," Phys. Rev. D **53**, 6203 (1996).

[50] E. Braaten, S. Fleming and A. K. Leibovich, "NRQCD analysis of bottomonium production at the Tevatron," Phys. Rev. D **63**, 094006 (2001).

[51] H. L. Lai, M. Guzzi, J. Huston, Z. Li, P. M. Nadolsky, J. Pumplin and C.-P. Yuan, "New parton distributions for collider physics," Phys. Rev. D **82**, 074024 (2010),

[52] K. Nakamura *et al.* [Particle Data Group Collaboration], "Review of particle physics," J. Phys. G **37**, 075021 (2010).

[53] E. J. Eichten and C. Quigg, "Mesons with beauty and charm: Spectroscopy," Phys. Rev. D **49**, 5845 (1994).

[54] M. Beneke and M. Kramer, 1, "Direct J/ψ and ψ' polarization and cross-sections at the Tevatron," Phys. Rev. D **55**, 5269 (1997), [hep-ph/9611218].